Electronic Supplementary Material (ESI) for ChemComm.

Supporting Information

Stable Bis(trifluoromethyl)Nickel(III) Complexes

Fengzhi Tang,[†] Nigam P. Rath,[‡] and Liviu M. Mirica*,[†]

[†]*Department of Chemistry, Washington University, One Brookings Drive, St. Louis, Missouri 63130-4899*

and [‡]*Department of chemistry and Biochemistry, University of Missouri-St. Louis, One University Boulevard, St. Louis, Missouri 63121-4400.*

Table of Contents

I. General specifications

All operations were performed under a nitrogen atmosphere using standard Schlenk and glove box techniques if not indicated otherwise. All reagents for which the syntheses are not given were purchased from Fisher Scientific, Sigma-Aldrich, Acros, STREM, or Pressure Chemical and were used as received without further purification. Solvents were purified prior to use by passing through a column of activated alumina using an MBRAUN SPS. $(CH_3CN)Ni^{II}(CF_3)_2$ was prepared according to literature procedures.[1] ^1H (300 MHz), ^{13}C, and ^{19}F NMR spectra were obtained on a Varian Mercury-300 spectrometer. Chemical shifts are reported in parts per million (ppm) with residual solvent resonance peaks as internal references.[2] Abbreviations for the multiplicity of NMR signals are singlet (s), doublet (d), triplet (t), quartet (q), septet (sep), multiplet (m), broad resonance (br). Solution magnetic susceptibility measurements were obtained by the Evans method[3] in MeCN using coaxial NMR tubes at 293 K, and diamagnetic corrections were applied as previously described.[4] UV-vis spectra were recorded on a Varian Cary 50 Bio spectrophotometer and are reported as λ_{max}, nm (ε, $M^{-1}cm^{-1}$). EPR spectra were recorded on a JEOL JES-FA X-band (~9.2 GHz) EPR spectrometer in 3:1 PrCN:MeCN at 77 K or 293 K. ESI-MS experiments were performed using a linear quadrupole ion trap Fourier transform ion cyclotron resonance mass spectrometer (LTQ-FTMS, Thermo, San Jose, CA) or a Bruker Maxis Q-TOF mass spectrometer with an electrospray ionization source. ESI mass-spectrometry was provided by the Washington University Mass Spectrometry Resource. Elemental analyses were carried out by the Columbia Analytical Services Tucson Laboratory and Intertek Pharmaceutical Services.

Electrochemical measurements

Cyclic voltammetry (CV) studies were performed with a BASi EC Epsilon electrochemical workstation or CHI Electrochemical Analyzer 660D. Electrochemical grade Bu_4NClO_4 from Fluka were used as the supporting electrolytes. The electrochemical measurements were performed under a blanket of nitrogen, and the analyzed solutions were deaerated by purging with nitrogen. A glassy carbon disk electrode (GCE) was used as the working electrode, and a Pt wire as the auxiliary electrode. The non-aqueous Ag-wire reference electrode assembly was filled with 0.01 M $AgNO_3$/0.1 M Bu_4NClO_4/MeCN solution. The reference electrodes were calibrated against ferrocene at the end of each CV measurement.

II. Synthesis of Ni complexes

Synthesis of (^{Me}N4)Ni^{II}(CF$_3$)$_2$. $(CH_3CN)_2Ni^{II}(CF_3)_2$ (84.5 mg, 0.30 mmol) and ^{Me}N4 ligand (81.3 mg, 0.30 mmol) were dissolved in 5 mL dry THF. The mixture was stirred at room temperature for 2h and the precipitate was isolated, further washed with pentane, and dried under vacuum (135.3 mg, yield 96%).

^{1}H NMR (300 MHz, CD_3CN): 7.48 (t, 2H, J = 7.5 Hz, Py-H), 7.02 (d, 2H, J = 7.5 Hz, Py-H), 6.96 (d, 2H, J = 7.5 Hz, Py-H), 6.68 (d, 2H, J = 14.1 Hz, -CH_2-), 4.69 (d, 2H, J = 16.5 Hz, -CH_2-), 4.37 (d, 2H, J = 13.8 Hz, -CH_2-), 4.10 (d, 2H, J = 16.5 Hz, -CH_2-), 3.48 (s, 9H, N-CH_3), 2.29 (s, 9H, N-CH_3).

^{19}F NMR (CD_3CN): -23.77 ppm.

^{13}C NMR (151 MHz, DMSO-d_6): 158.1, 156.2, 137.2, 133.4 (q, J_F = 367 Hz), 124.6, 121.4, 64.6, 63.5, 48.0, 37.8. Note: The quality of the ^{13}C NMR spectrum is less than optimal due to the poor solubility of the complex.

ESI-MS of (^{Me}N4)Ni^{II}(CF$_3$)$_2$ in MeCN, m/z 395.0986. Calcd for [(^{Me}N4)Ni^{II}CF$_3$]$^+$ ($C_{17}H_{20}F_3N_4Ni$) 395.0884. In addition, a lpeak at m/z 464.0968 was observed that corresponds to [(^{Me}N4)Ni^{III}(CF$_3$)$_2$]$^+$, suggesting that the Ni(II) complexes undergoes rapid oxidation to the Ni(III) complex under MS conditions.

The (^{Me}N4)Ni^{II}(CF$_3$)$_2$ complex is very air sensitive and no satisfactory elemental analysis could be obtained despite several attempts.

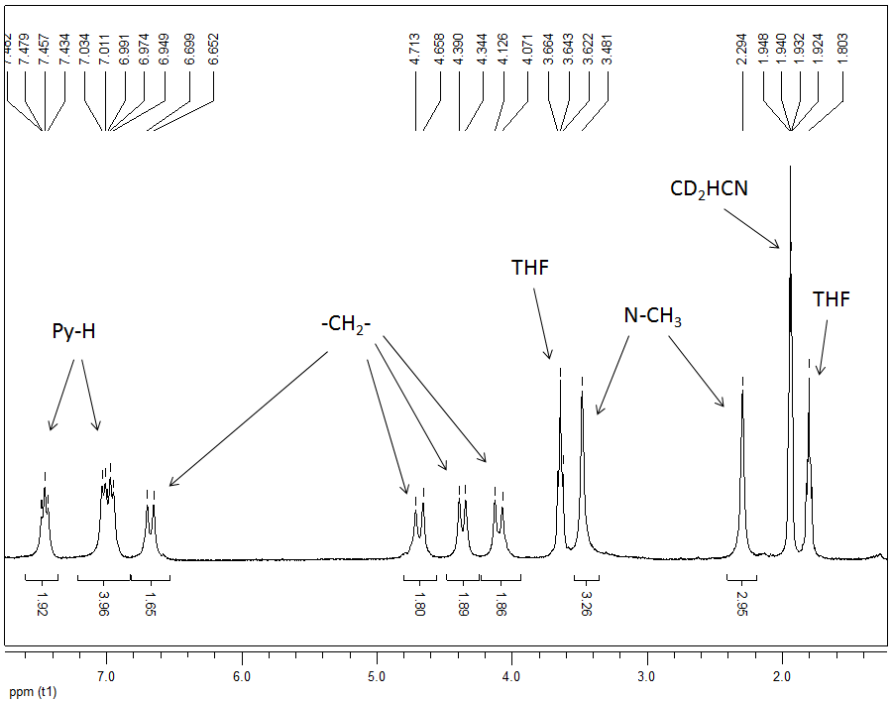

Figure S1. ^{1}H NMR spectrum of (^{Me}N4)Ni^{II}(CF$_3$)$_2$ in CD$_3$CN.

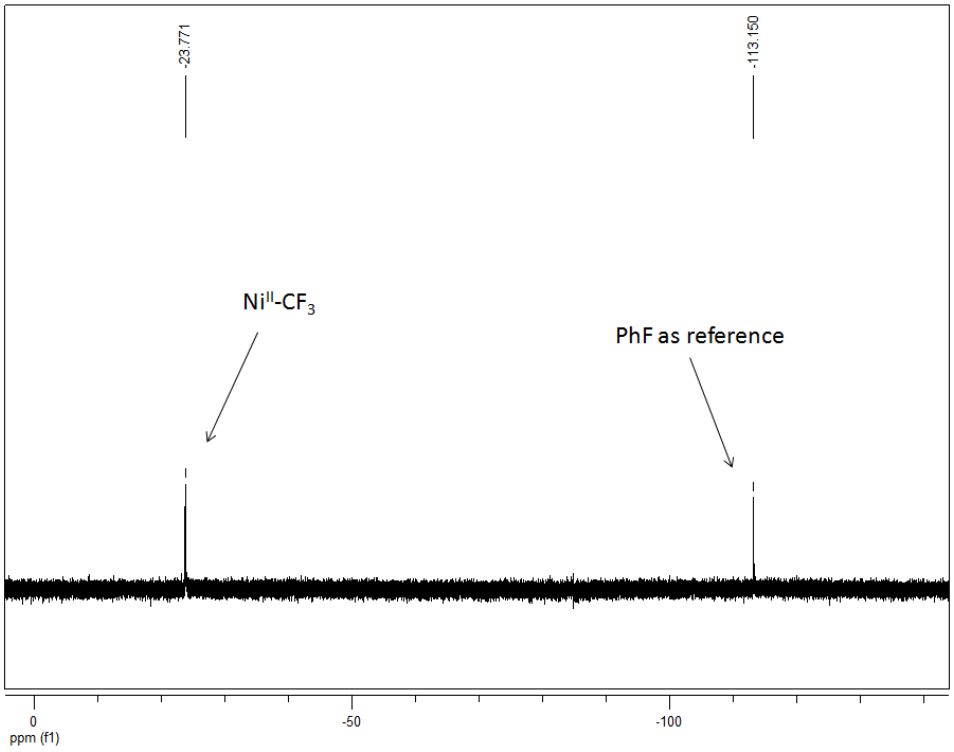

Figure S2. ^{19}F NMR spectrum of (^{Me}N4)Ni^{II}(CF$_3$)$_2$ in CD$_3$CN (fluorobenzene was added as reference).

Synthesis of [(^{Me}N4)Ni^{III}(CF$_3$)$_2$]PF$_6$ ([1$^+$]PF$_6$). (^{Me}N4)Ni^{II}(CF$_3$)$_2$ (0.029 mmol, 13.3 mg) was dissolved in 3 mL CH$_3$CN, 1 equiv FcPF$_6$ (0.029 mmol 13.3 mg) was added and the reaction stirred for 30 min at RT. After filtration, the filtrate was extracted with pentane (3 x 5 mL) to remove FcPF$_6$, the MeCN layer was dried under vacuum to generate 14.6 mg of dark purple solid (yield 84%). Evans method: μ_{eff} = 2.06 μ_B. No CF$_3$ peaks were observed in ^{19}F NMR likely due to the paramagnetic Ni(III) center.

UV-Vis in MeCN: 568 nm (330), 680 (shoulder).

ESI-MS (MeCN): found for [(^{Me}N4)Ni^{III}(CF$_3$)$_2$]PF$_6$, m/z 464.0946. Calcd. for C$_{18}$H$_{20}$F$_6$N$_4$Ni: 464.0946.

^{1}H NMR (300 MHz, CD$_3$CN): 11.81, 11.51, 7.82, 7.32, 4.28. Note: the ^{1}H NMR of the paramagnetic complex **1**$^+$ shows broad and unintegratable peaks.

Anal. Found: C, 35.32; H, 3.08; N, 8.62. Calcd for C$_{18}$H$_{20}$F$_{12}$N$_4$NiP: C, 35.44; H, 3.30; N, 9.18.

Synthesis of (^{tBu}N4)Ni^{II}(CF$_3$)$_2$ (2). (CH$_3$CN)$_2$Ni^{II}(CF$_3$)$_2$ (52.3 mg, 0.19 mmol) and ^{tBu}N4 (66.1 mg, 0.19 mmol) were dissolved in 5 mL dry THF. The mixture was stirred at room temperature for 2 h and filtered. Then 15 mL of dry pentane was added to the filtrate slowly and the mixture was stored at -35 ºC overnight to yield a yellow solid. The solid was further washed with pentane and dried under vacuum (60 mg, yield 54%).

^{1}H NMR (300 MHz, CD$_3$CN): 7.51 (t, 2H, *J* = 7.8 Hz, Py-H), 7.11 (d, 2H, *J* = 7.5 Hz, Py-H), 7.00 (d, 2H, *J* = 7.5 Hz, Py-H), 6.53 (d, 2H, *J* = 14.4 Hz, -CH$_2$-), 4.95 (d, 2H, *J* = 16.2 Hz, -CH$_2$-), 4.86 (d, 2H, *J* = 14.4 Hz, -CH$_2$-), 3.70 (d, 2H, *J* = 14.4 Hz, -CH$_2$-) 1.67 (s, 9H, ^{t}Bu), 1.37 (s, 9H, ^{t}Bu).

^{19}F NMR (300 MHz, CD$_3$CN): -23.47 (s, CF$_3$).

^{13}C NMR (151 MHz, DMSO-*d*$_6$): 162.6, 159.6, 138.3, 123.6, 121.3, 61.1, 58.0, 57.4, 56.3, 27.7, 26.1. Note: The quality of the ^{13}C NMR spectrum is less than optimal due to the poor solubility of the complex.

ESI-MS of (^{tBu}N4)Ni^{II}(CF$_3$)$_2$ in MeCN, m/z 548.1903; Calcd for [(^{tBu}N4)Ni^{III}(CF$_3$)$_2$)]$^+$, C$_{24}$H$_{32}$F$_6$N$_4$Ni, 548.1885. Note: the Ni^{II} complex was partially oxidized to the Ni^{III} species under the ESI-MS conditions.

Anal. Found: C, 52.26; H, 5.36; N, 9.96. Calcd for C$_{24}$H$_{32}$F$_6$N$_4$Ni C, 52.48; H, 5.87; N, 10.20.

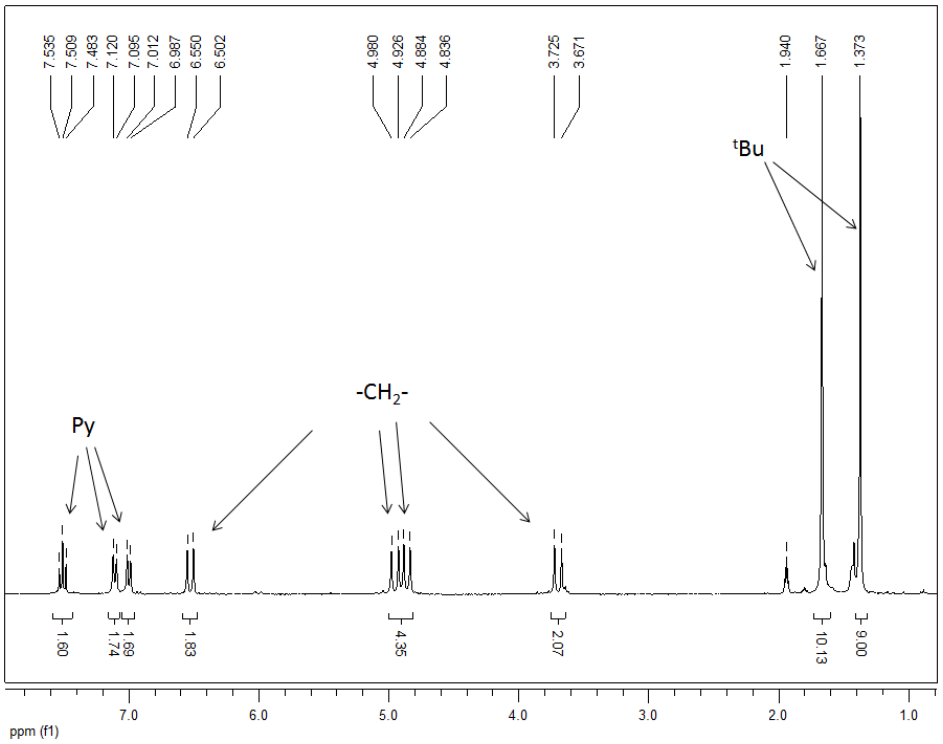

Figure S3. ^{1}H NMR spectrum of (^{tBu}N4)Ni^{II}(CF$_3$)$_2$ in CD$_3$CN.

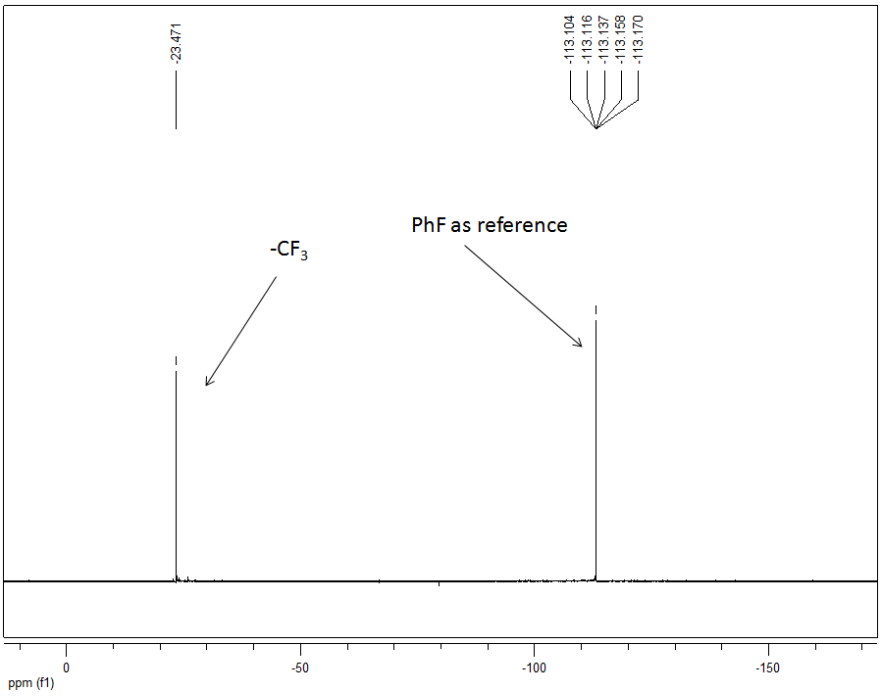

Figure S4. ^{19}F NMR spectrum of (^{tBu}N4)Ni^{II}(CF$_3$)$_2$ in CD$_3$CN (fluorobenzene was added as reference).

Synthesis of [(^{tBu}N4)Ni^{III}(CF$_3$)$_2$]PF$_6$ ([2$^+$]PF$_6$). (^{tBu}N4)Ni^{II}(CF$_3$)$_2$ (19.3 mg, 0.04 mmol) and 1 equiv FcPF$_6$ (11.6 mg, 0.04 mmol) were mixed in 2 mL of THF at - 50 ºC to generate an orange precipitate within a few minutes. The suspension was stirred for 3 hours, and then allowed to stand at - 35 ºC overnight. The precipitate was filtered, washed with pentane, and dried to give 18.0 mg of an orange solid (yield 65%). Evans method (CD$_3$CN): μ_{eff} = 2.15 μ_b. No CF$_3$ peaks was observed in ^{19}F NMR likely due to the paramagnetic Ni(III) center.

UV-Vis in MeCN: 422 nm (930), 930 nm (40).

ESI-MS of [(^{tBu}N4)Ni^{III}(CF$_3$)$_2$]PF$_6$ in MeCN, m/z 548.1906; calculated for [(^{tBu}N4)Ni^{III}(CF$_3$)$_2$)]$^+$, C$_{24}$H$_{32}$F$_6$N$_4$Ni, 548.1885.

^{1}H NMR (300 MHz, CD$_3$CN): 14.32, 10.49, 8.86, 7.77, 3.64, 1.24. Note: the ^{1}H NMR of the paramagnetic complex **2**$^+$ shows broad and unintegratable peaks.

Anal. Found: C, 44.08; H, 5.55; N, 7.04. Calcd for $[(^{tBu}N4)Ni^{III}(CF_3)_2]PF_6 \cdot THF$, ($C_{28}H_{40}F_{12}N_4NiOP$): C, 43.89; H, 5.26; N, 7.31.

III. Cyclic voltammograms of Ni complexes

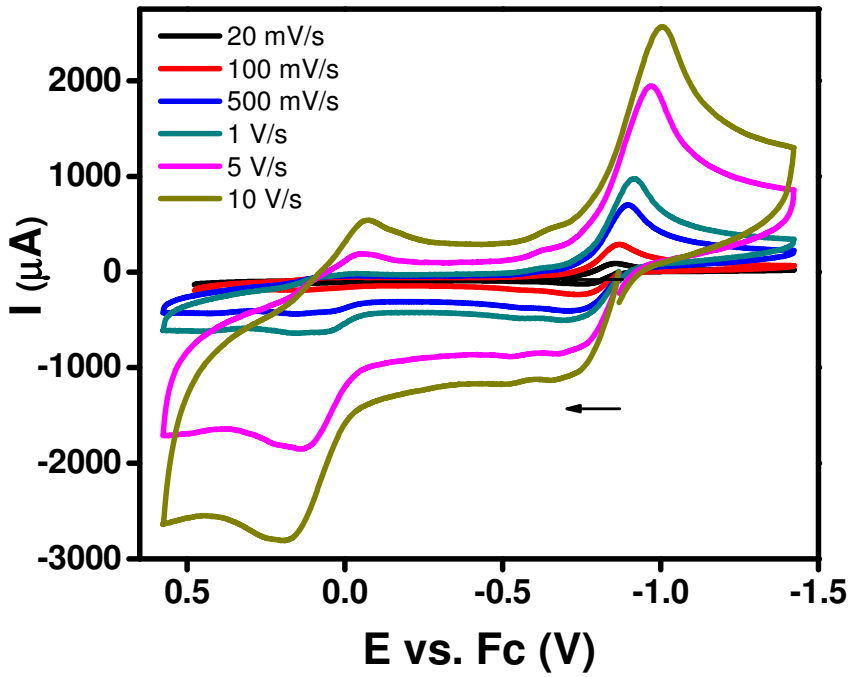

Figure S5. Cyclic voltammograms of (^{Me}N4)Ni^{II}(CF$_3$)$_2$ (**1**) in 0.1M Bu$_4$NClO$_4$/CH$_3$CN at various scan rates.

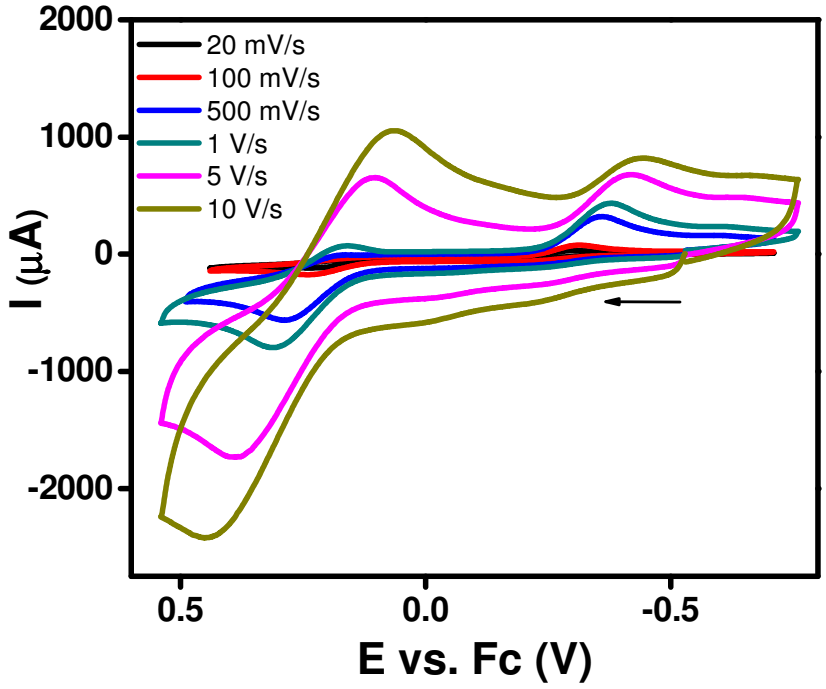

Figure S6. Cyclic voltammograms of (^{tBu}N4)Ni^{II}(CF$_3$)$_2$ (**2**) in 0.1M Bu$_4$NClO$_4$/CH$_3$CN at various scan rates.

IV. UV-Vis spectra of Ni complexes

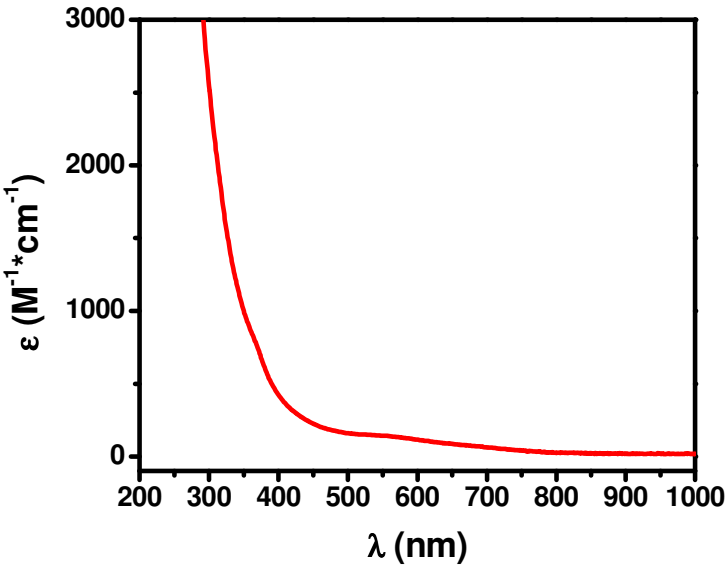

Figure S7. UV-vis spectrum of (^{Me}N4)Ni^{II}(CF$_3$)$_2$ in MeCN.

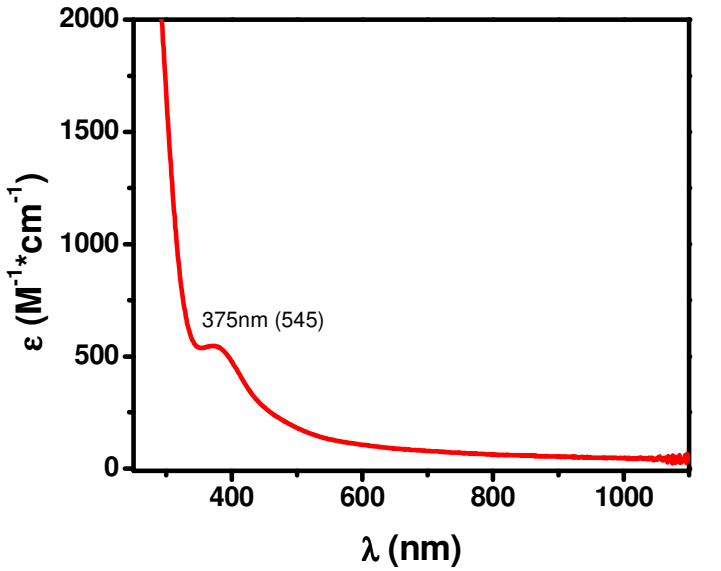

Figure S8. UV-vis spectrum of (^{tBu}N4)Ni^{II}(CF$_3$)$_2$ in MeCN.

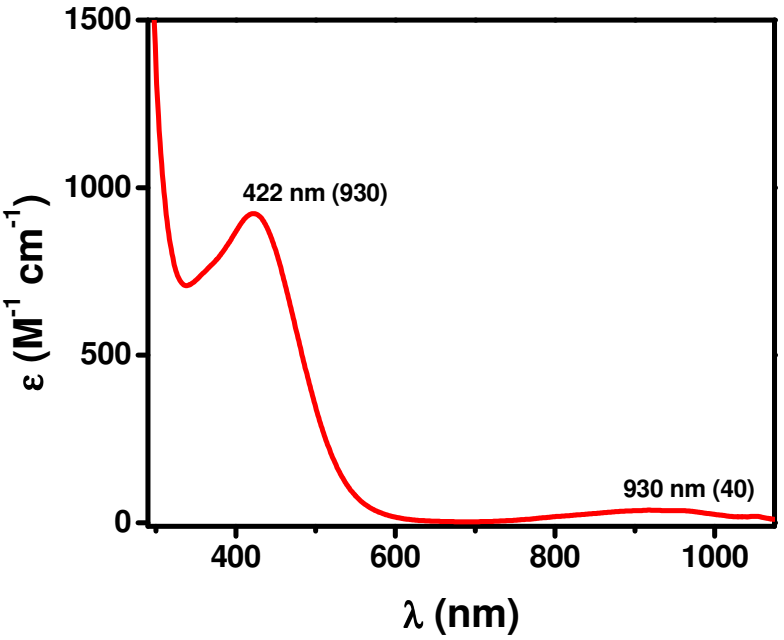

Figure S9. UV-vis spectrum of [(^{tBu}N4)Ni^{III}(CF$_3$)$_2$]PF$_6$ in MeCN.

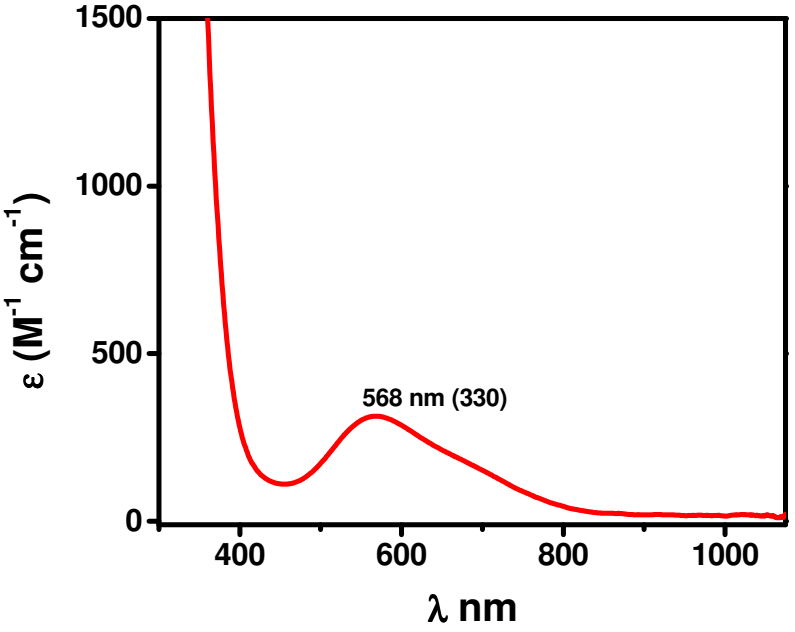

Figure S10. UV-vis spectrum of [(^{Me}N4)Ni^{III}(CF$_3$)$_2$]PF$_6$ in MeCN.

V. Reactivity studies of Ni complexes

About 10 mg of [(^{Me}N4)Ni^{III}(CF$_3$)$_2$](PF$_6$), [**1**$^+$]PF$_6$, and [(^{tBu}N4)Ni^{III}(CF$_3$)$_2$](PF$_6$), [**2**$^+$]PF$_6$, were dissolved in degassed d$_6$-DMSO and the NMR tubes were filled to the top to avoid the escape of the volatiles into the headspace. The NMR tubes were then sealed with rubber septa and parafilmed. For photolysis studies, the NMR tubes were placed in an 25 ^{o}C water bath and irradiated with two 100 W halogen lamps placed at a distance about 10 cm from the sample. For thermolysis studies, the NMR tubes were placed in a 100 ^{o}C mineral oil bath. Fluorobenzene (1 equiv) was added to the NMR sample as an internal standard. The reactions were monitored for 24 h, and no precipitate formed during one day for either photolysis or thermolysis reactions. For the photolysis study of [(^{tBu}N4)Ni^{III}(CF$_3$)$_2$]BF$_4$, 5 equiv of the spin trap *N-tert*-butyl-α-phenylnitrone (PBN) was added in order to probe the formation of the trifluoromethane radical and its role in product formation. The organic products such CF_3H and CF_3CF_3 were identified by comparison of ^{19}F NMR with literature reported data.[5] Product yields (Table S1) were determined by intergration of the corresponding NMR peaks relative to the fluorobenzene standard and calculated as [moles of product]/[moles of internal standard]*100%.

Control photolysis and thermolysis studies using the Ni^{II} precursors (^{Me}N4)Ni^{II}(CF$_3$)$_2$ and (^{tBu}N4)Ni^{III}(CF$_3$)$_2$ reveals formation of negligible amounts of CF_3H and CF_3CF_3 (less than 1%).

Table S1. Product yields for the photolysis and thermolysis studies of [(^{Me}N4)Ni^{III}(CF$_3$)$_2$]$^+$ (**1**$^+$) and [(^{tBu}N4)Ni^{III}(CF$_3$)$_2$]$^+$ (**2**$^+$).

Product	**1**$^+$ [a]	**1**$^+$ [b]	**2**$^+$ [a]	**2**$^+$ [b]	**2**$^+$ [c]
CF_3H	ND	2 %	5 %	7.4 %	5 %
CF_3CF_3	ND	ND	1.4 %	2 %	ND

[a] thermolysis; [b] photolysis; [c] photolysis in the presence of 5 equiv PBN. ND – not detected.

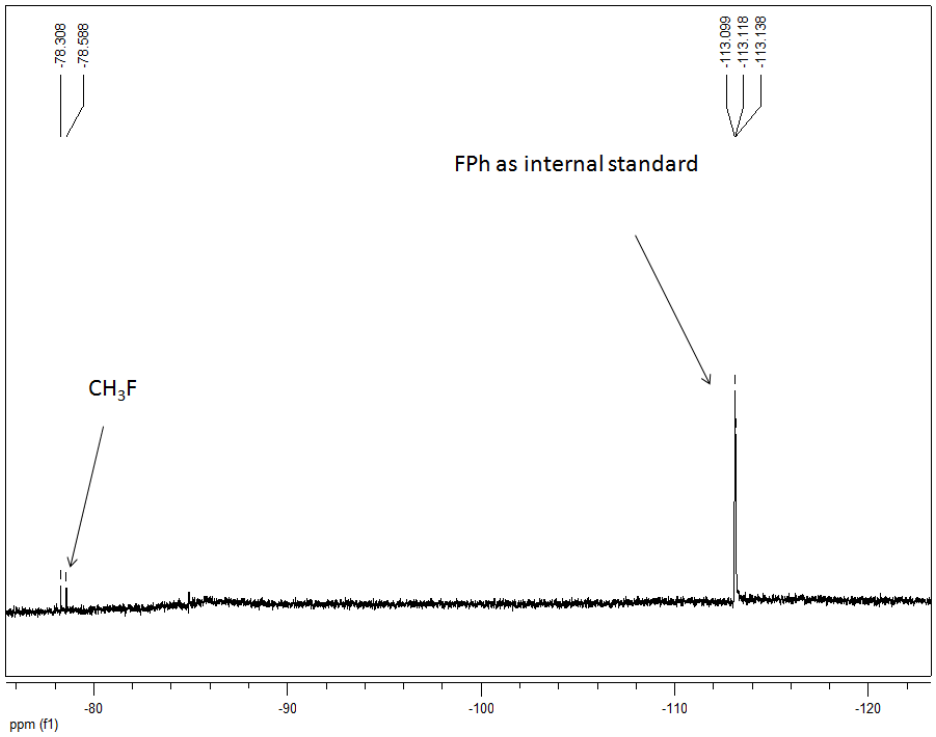

Figure S11. ^{1}H NMR spectrum of photolysis of [**1**$^{+}$]BF_4 in DMSO at 100 ^{o}C after 24 h.

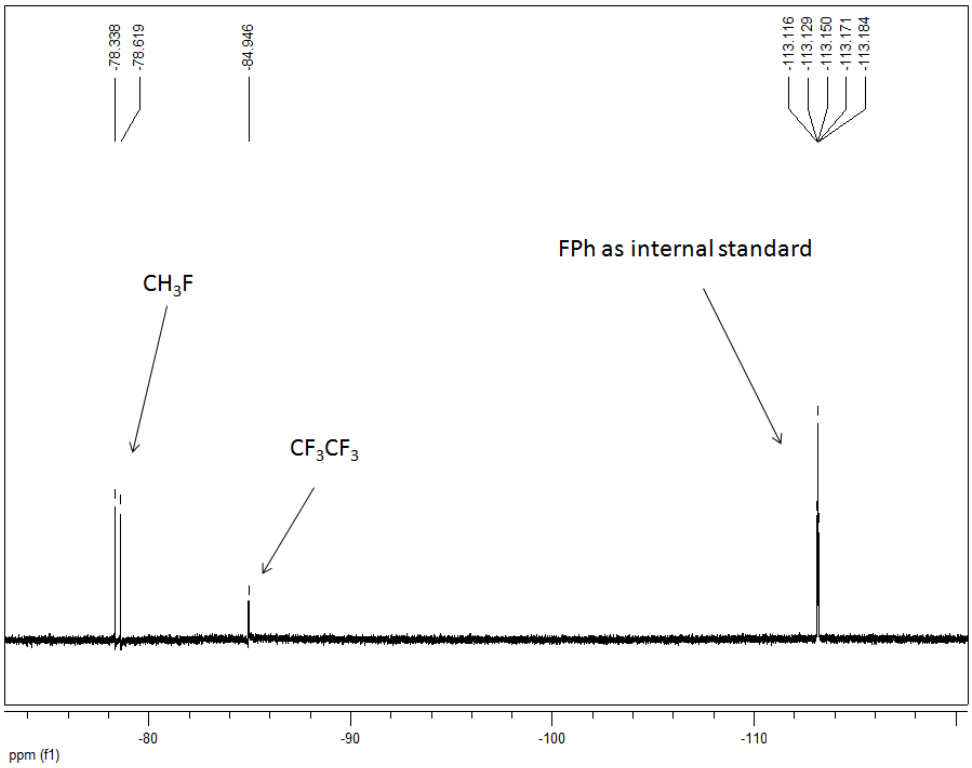

Figure S12. ^{1}H NMR spectrum of thermolysis of [**2**$^{+}$]BF_4 in DMSO at 100 ^{o}C after 24 h.

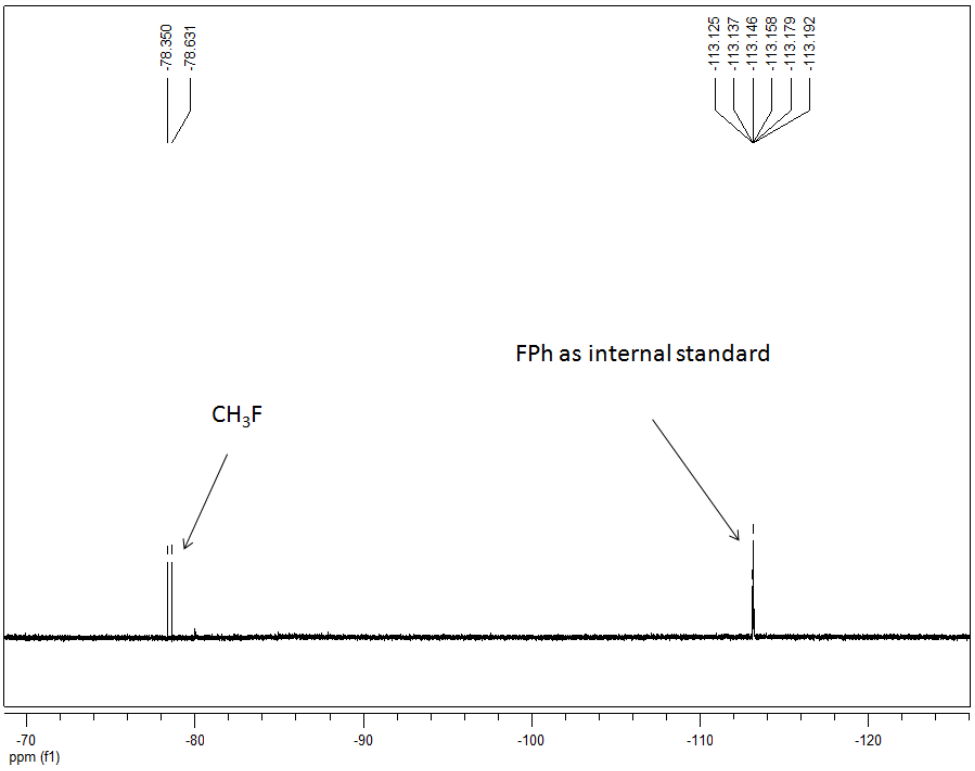

Figure S13. ^{1}H NMR spectrum of photolysis of [**2**$^{+}$]BF_4 in DMSO at 25 ^{o}C after 24 h.

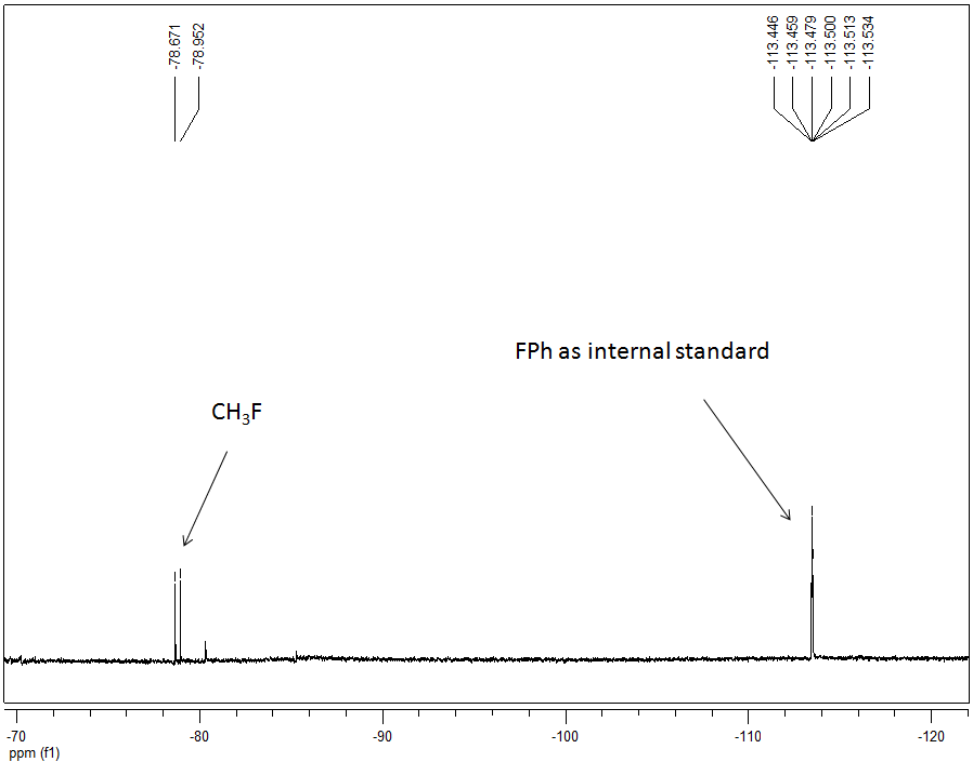

Figure S14. ^{1}H NMR spectrum of photolysis of [**2**$^{+}$]BF_4 with 5 equiv. of PBN in DMSO at 25 ^{o}C after 24 h.

PBN spin trapping EPR studies

13.3 mg of $[(^{tBu}N4)Ni^{III}(CF_3)_2]BF_4$ and 12.3 mg *N-tert*-butyl-α-phenylnitrone (PBN) were dissolved in 2 mL of DMSO solution in an NMR tube. The concentrations of $[(^{tBu}N4)Ni^{III}(CF_3)_2]BF_4$ and PBN were 9.5 mM and 50 mM, respectively. After 24 hours of irradiation at 25 °C, 100 µL of the reaction mixture was transferred to a thin EPR tube and the EPR spectrum was recorded immediately at RT. The parameters for the simulated spectrum are similar to those reported previously for the PBN-CF_3 adduct.[1] In addition, the amount of the PBN-CF_3 adduct was quantified as being ~5% by spin integration and comparison with the spin integration corresponding to a 1 mM TEMPO solution under the same experimental conditions.

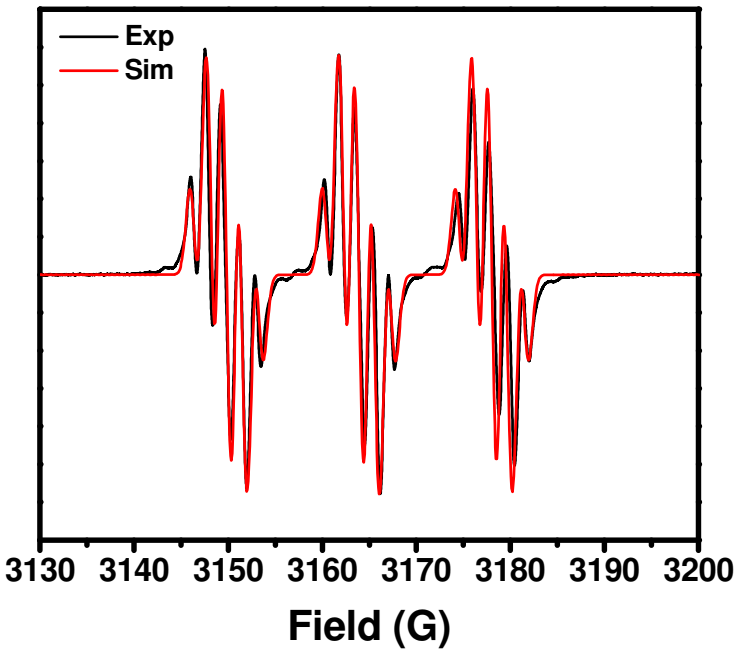

Figure S15. EPR spectrum of $[(^{tBu}N4)Ni^{III}(CF_3)_2]BF_4$ in presence of 5 equiv. PBN after 16 hours of photolysis in NMR tube (293 K). Parameters used for simulation: g = 2.0052, A_N = 14.10 G, A_H = 1.20 G, $A_F(CF_3)$ = 1.85 G, linewidth = 1.10 G.

Aerobic oxidation reactivity of (^{Me}N4)Ni^{II}(CF$_3$)$_2$ (1)

A 3.0 mM solution of (^{Me}N4)Ni^{II}(CF$_3$)$_2$ (**1**) in 5% H$_2$O/MeCN solution was placed into a quartz cuvette (pathlength 1.0 cm) equipped with a septum-sealed cap and a magnetic stir bar. O$_2$ was bubbled through the solution for about 2 min and then reaction mixture was stirred under O$_2$ at 20 °C in the dark. The reaction was monitored using a Varian Cary 50 Bio spectrophotometer (Figure S16). During the oxidation, the initial pale yellow solution turned purple with an absorption band at 568 nm, identical to that of the independently prepared [(^{Me}N4)Ni^{II}(CF$_3$)$_2$]PF$_6$ ([**1**$^+$]PF$_6$). The concentration of **1**$^+$ was calculated using the extinction coefficient of the 568 nm absorption band (ε = 330 M^{-1} cm^{-1}). The yield of [(^{Me}N4)Pd^{III}Me$_2$]$^+$ is calculated as ([**1**$^+$]/ [**1**]$_{initial}$)*100%. The maximum concentration of [(^{Me}N4)Pd^{III}Me$_2$]$^+$ of ~2.4 mM was reached after 10 min (~80 % yield). The identity of **1**$^+$ was confirmed by EPR (Figure S17) and ESI-MS (found m/z: 464.0946, calculated for C$_{18}$H$_{20}$F$_6$N$_4$Ni: 464.0946).

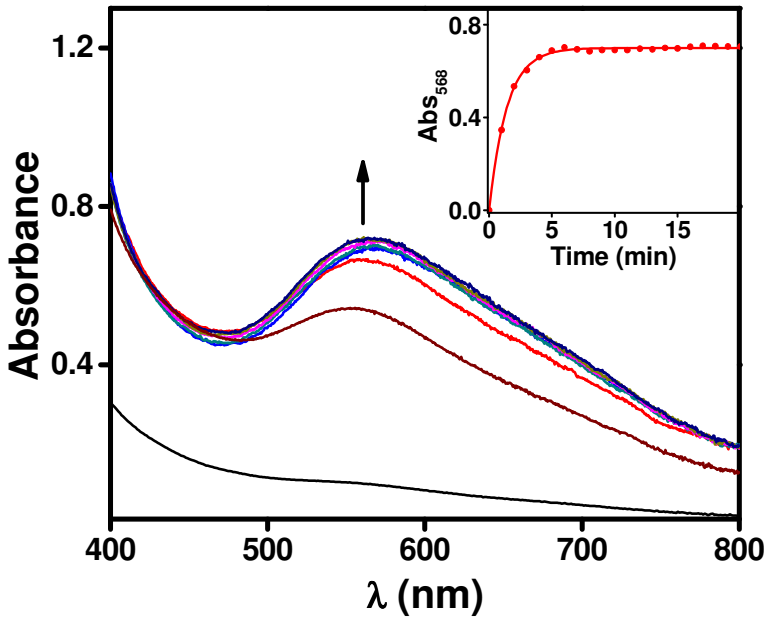

Figure S16. Formation of **1**$^+$ during aerobic oxidation of **1** (3.0 mM) in 5% H$_2$O/MeCN, monitored by UV-vis spectroscopy (Δt = 5 min). Inset: time course of the formation **1**$^+$ upon aerobic oxidation of **1**, and the first-order fit of the absorption data at 568 nm to yield a first-order rate constant of 0.71 ± 0.02 min^{-1} (R = 0.999).

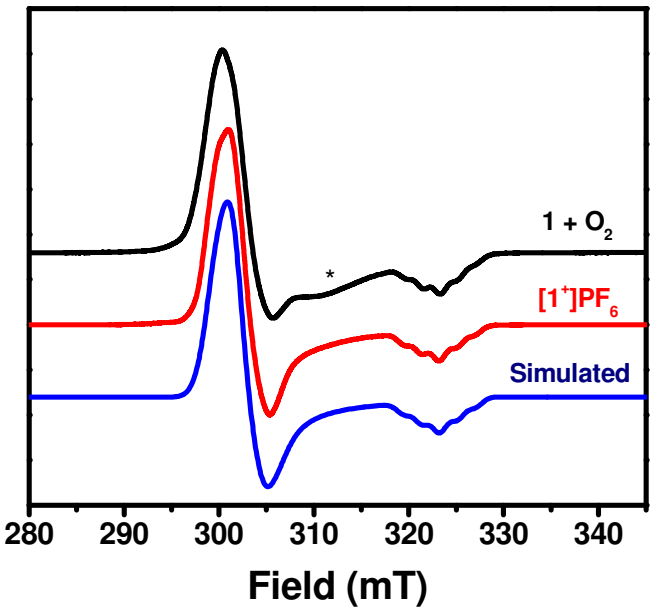

Figure S17. EPR spectra of the product of oxidation of **1** with O_2 in 5% H_2O/MeCN and diluted 3 time in PrCN (black line), a solution of isolated [**1**$^+$]PF_6 in 3:1 PrCN:MeCN (red line), and a simulated EPR spectrum (blue line) using the following parameters: g_x = 2.154 (A_N = 10.0 G); g_y = 2.152 (A_N = 16.0 G); g_z = 2.011 (A_N = 18.5 G). The feature marked with an asterisk is likely due to the presence of H_2O and OH^- in the solution.

<u>*Note*</u>: Under identical conditions, the aerobic oxidation of (^{tBu}N4)$Ni^{II}(CF_3)_2$ (**2**) also occurs, albeit at a much lower rate, in line with the higher oxidation potential of **2** vs. **1**.

VI. Computational details

The density functional theory (DFT) calculations were performed with the program package Gaussian 09.[6] Single point and geometry optimization calculations were performed using the B3LYP functional along with the m6-31G* basis set. This functional/basis set combination has been shown previously to reproduce well experimental parameters of organometallic Ni complexes.[1,7] Geometry optimization calculations were performed using the crystallographic coordinates for $\mathbf{1}^{+}$ and $\mathbf{2}^{+}$ as the starting geometries. The calculated ground state wavefunctions were investigated by analyzing the frontier molecular orbitals (Tables S3 and S4) and the atomic contributions to the spin density (Table S2) calculated using the program Chemissian (http://www.chemissian.com). TD-DFT calculations were employed to obtain the predicted absorption bands and their major contributions transitions (Tables S5 and S6). The calculated UV-vis spectra were generated using the program GaussSum (http://gausssum.sourceforge.net), with a full width at half maximum (FWHM) value of 2,500 cm^{-1} (Figures S19 and S20). For the calculation of the EPR parameters of $\mathbf{1}^{+}$ and $\mathbf{2}^{+}$ (Table S7), the ORCA software package was employed in order to account for the spin-orbit coupling contribution to the g-tensor values and superhyperfine coupling constants.[8]

Optimized cartesian coordinates for **1**$^{+}$:

Ni	0.00000000	0.00000000	0.00000000
N	1.97896520	0.00000000	0.00000000
N	0.21035205	1.94599729	0.28998153
N	0.35661729	0.00000000	2.24296785
N	0.36602500	0.64347258	-2.14674262
C	-1.93914768	0.13003392	-0.13217937
C	-0.09997577	-1.94076994	-0.13613032
F	-2.31546719	1.34833306	-0.63627206
F	-2.55012768	-0.77358595	-0.94967229
F	-2.58238790	0.03189861	1.06842614
F	-0.08469131	-2.40661720	-1.41972347
F	0.98106470	-2.53038444	0.46686661
F	-1.17686578	-2.53188219	0.45492984
C	2.62939727	0.02594973	1.17385357
C	4.00275659	0.26367172	1.21869635
H	4.51660304	0.28591721	2.17402386
C	4.68629381	0.48104818	0.02349404
H	5.75476618	0.67364579	0.03407805
C	1.81177470	-0.27853332	2.40540731
H	1.92011651	-1.34788346	2.61004579
H	2.21538686	0.25696944	3.27314061
C	-0.40835825	-0.94159940	3.09691631
H	-0.17844164	-1.96596129	2.80307279
H	-1.47444496	-0.76278617	2.96585513
H	-0.14684873	-0.80651874	4.15542527
C	0.33126503	2.39432989	1.55296436
C	0.68981437	3.71529973	1.80728320
H	0.78124420	4.06430750	2.83022075
C	0.93926160	4.56155761	0.72572874
H	1.22873347	5.59395749	0.89677997
C	0.00496328	1.39319241	2.63164172
H	-1.07712881	1.41655339	2.79663822
H	0.48836247	1.67106543	3.57637535
C	2.61660308	0.23354569	-1.16189407
C	3.98777275	0.47264801	-1.18492120
H	4.48910523	0.65919855	-2.12855398
C	1.75540374	0.17145812	-2.39742234
H	1.68713682	-0.87597783	-2.70879265

H	2.21806960	0.73070952	-3.21990787
C	-0.51771682	0.11984938	-3.21728629
H	-0.47827777	-0.96821474	-3.21727201
H	-1.54240245	0.44135142	-3.02964068
H	-0.20064991	0.49318421	-4.20070480
C	0.46882224	2.73797909	-0.76241380
C	0.83708818	4.06978114	-0.57450118
H	1.04656311	4.69903186	-1.43321085
C	0.27148545	2.13092002	-2.13015000
H	-0.73629162	2.39965356	-2.46095741
H	0.97310034	2.57317250	-2.84767074

Optimized cartesian coordinates for **2**$^{+}$:

Ni	0.00000000	0.00000000	0.00000000
N	1.96482373	0.00000000	0.00000000
N	0.07957770	1.96325515	-0.00000000
N	0.58635315	0.41709146	2.37721055
N	0.43299991	0.56414696	-2.37310061
C	-1.96324487	0.01087233	0.08189729
C	-0.06182862	-1.96251997	-0.07471671
F	-2.52457440	-0.92729128	0.89640665
F	-2.55746528	-0.16934802	-1.13039270
F	-2.46173810	1.20456583	0.53062750
F	-0.25034740	-2.54304142	1.14321978
F	1.11011986	-2.50447822	-0.53132480
F	-1.02640829	-2.49493830	-0.87639855
C	2.61343775	-0.32902652	1.13392493
C	3.99825455	-0.48076998	1.14123951
H	4.50657238	-0.73754222	2.06449111
C	4.70260204	-0.28742858	-0.04648570
H	5.78009164	-0.41939627	-0.07129710
C	4.01866471	0.12004175	-1.19001111
H	4.54483115	0.33303366	-2.11458040
C	2.63471832	0.28358790	-1.13109493
C	1.87601483	0.93797698	-2.26161706
H	1.95258307	2.01748791	-2.09095527
H	2.41250011	0.75744988	-3.19245947
C	-0.41288413	1.79412585	-2.38264922
H	-1.45786218	1.49126792	-2.46296654
H	-0.18925147	2.43242910	-3.24439209
C	-0.22827782	2.62246399	-1.13394627
C	-0.32842062	4.01178594	-1.14252987
H	-0.56897736	4.52776587	-2.06586077
C	-0.10484622	4.71034655	0.04321256
H	-0.19615263	5.79204971	0.06607827
C	0.28027183	4.01345554	1.18659830
H	0.51507781	4.53265854	2.10981664
C	0.39096068	2.62416822	1.12935981
C	1.01704277	1.84332240	2.26043248
H	0.85902667	2.38773604	3.19103597
H	2.09858566	1.87905618	2.08802204

C	1.77942888	-0.47975934	2.38319539
H	2.42752721	-0.28429634	3.24431044
H	1.43159750	-1.51081687	2.46128444
C	0.19097907	-0.28798426	-3.64079112
C	-1.25438226	-0.80657034	-3.69420067
H	-1.48480393	-1.43756247	-2.83836274
H	-1.36207071	-1.40914108	-4.60256041
H	-1.99343619	-0.00321305	-3.75454939
C	0.45146680	0.52903436	-4.92914510
H	-0.29131319	1.31921032	-5.07663956
H	0.37913957	-0.14805980	-5.78698429
H	1.44752466	0.98234532	-4.95834197
C	1.12787296	-1.50907100	-3.62538806
H	2.18557677	-1.23937883	-3.69764692
H	0.89697238	-2.13068522	-4.49687377
H	0.98357132	-2.11717100	-2.73225276
C	-0.26881926	0.21394535	3.64877036
C	-0.83763517	-1.21186128	3.71210581
H	-1.46645045	-1.42904081	2.85131066
H	-1.45405499	-1.28997582	4.61428972
H	-0.06073541	-1.97750529	3.78958837
C	0.56328193	0.45191023	4.93190711
H	1.32516844	-0.31973487	5.07981937
H	-0.11120515	0.41163187	5.79371478
H	1.05646160	1.42917229	4.95236007
C	-1.45804613	1.19120323	3.62905059
H	-1.15562657	2.24151411	3.67990054
H	-2.07876248	0.99619076	4.50988056
H	-2.07897057	1.05132158	2.74380260

Table S2. Selected atomic contributions to Mulliken spin density for the ground state of $[(^{Me}N4)Ni^{III}(CF_3)_2]^+$, **1**$^+$, and $[(^{tBu}N4)Ni^{III}(CF_3)_2]^+$, **2**$^+$ (atomic coordinates taken from the X-ray structures).

1$^+$			**2**$^+$		
1	Ni	0.825674	1	Ni	0.849940
2	N_{eq}	0.008255	2	N_{eq}	0.006767
3	N_{eq}	0.008386	3	N_{eq}	0.006842
4	N_{ax}	0.096862	4	N_{ax}	0.092928
5	N_{ax}	0.096688	5	N_{ax}	0.093448
6	C	-0.018128	6	C	-0.022048
7	C	-0.018014	7	C	-0.022129

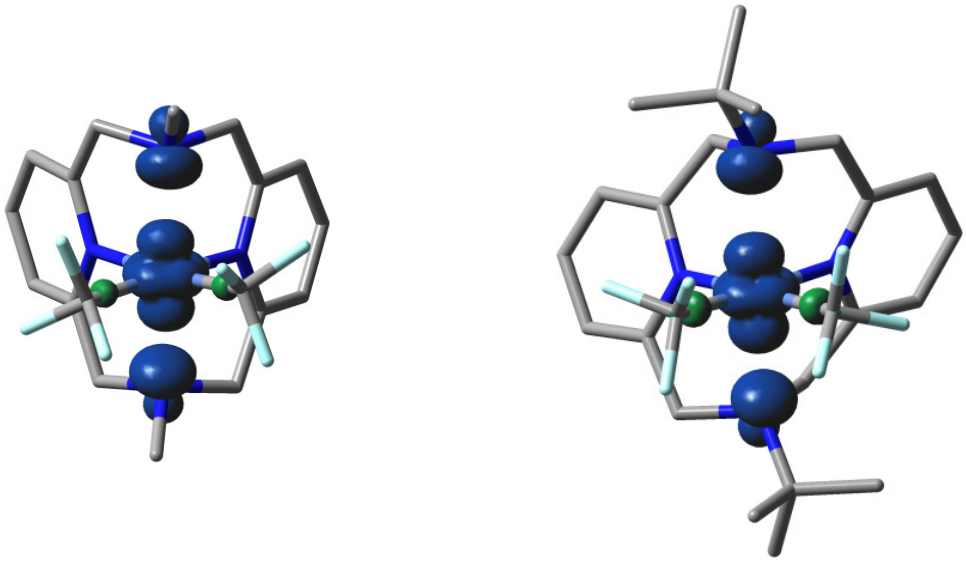

1$^+$ **2**$^+$

Figure S18. DFT calculated spin density for complexes $[(^{Me}N4)Ni^{III}(CF_3)_2]^+$, **1**$^+$, and $[(^{tBu}N4)Ni^{III}(CF_3)_2]^+$, **2**$^+$, shown as 0.005 isodensity contour plots.

Table S3. Isocontour plots and energies of frontier molecular orbitals for $[(^{Me}N4)Ni^{III}(CF_3)_2]^+$, **1**$^+$. The atomic contributions to the MOs are shown the Ni center, the Ni-bonded C atom of the CF_3 ligands, the axial N atoms (N_{ax}), and the equatorial N atoms (N_{eq}).

MO # Energy (eV)	MOs (0.05 isocontour value)	Atom Simple Distribution
β-HOMO-9 -8.893	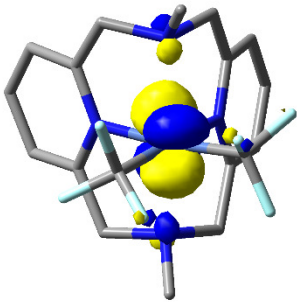	Ni 0.86 C_{CF3} 0.01 N_{eq} 0.01 N_{ax} 0.04
β-HOMO-8 -8.818	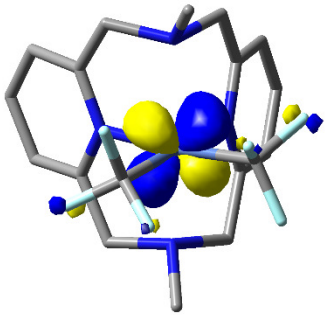	Ni 0.90 C_{CF3} 0.01 N_{eq} 0.01 N_{ax} 0.01
α-HOMO -6.226	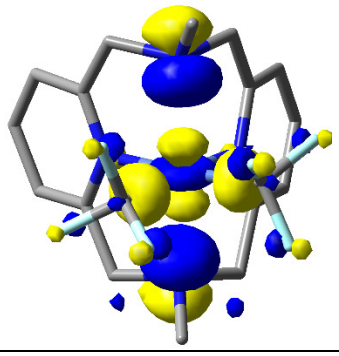	Ni 0.25 C_{CF3} 0.10 N_{eq} 0.02 N_{ax} 0.40
α-LUMO -2.252	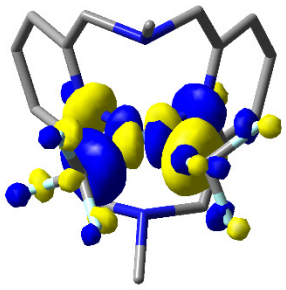	Ni 0.42 C_{CF3} 0.34 N_{eq} 0.12 N_{ax} 0.00

β-LUMO -2.420	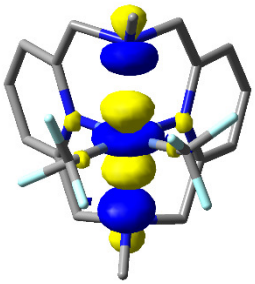	Ni 0.70 C_{CF3} 0.02 N_{eq} 0.02 N_{ax} 0.16

Table S4. Isocontour plots and energies of frontier molecular orbitals for $[(^{tBu}N4)Ni^{III}(CF_3)_2]^+$, **2**$^+$. The atomic contributions to the MOs are shown for the Ni center, the Ni-bonded C atom of the CF_3 ligands, the axial N atoms (N_{ax}), and the equatorial N atoms (N_{eq}).

MO # Evergy (eV)	MOs (0.05 isocontour value)	Atoms Simple Distribution
β-HOMO-12 -9.165	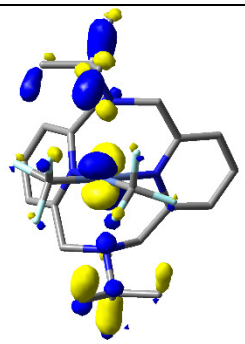	Ni 0.48 C_{CF3} 0.00 N_{eq} 0.00 N_{ax} 0.05
β-HOMO-4 -7.877	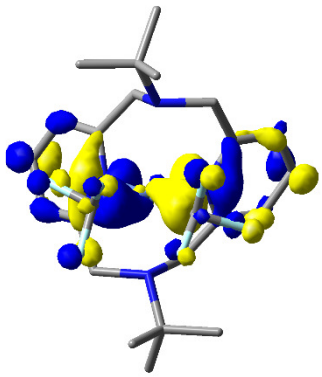	Ni 0.12 C_{CF3} 0.14 N_{eq} 0.28 N_{ax} 0.01
β-HOMO-2 -7.338	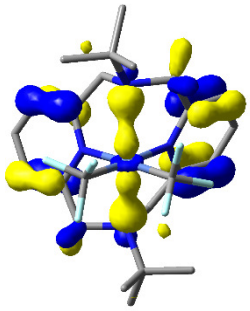	Ni 0.09 C_{CF3} 0.00 N_{eq} 0.00 N_{ax} 0.15
α-HOMO -6.559	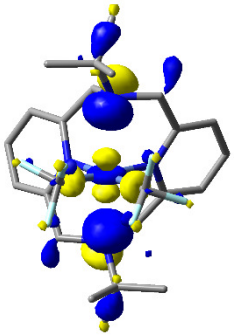	Ni 0.14 C_{CF3} 0.07 N_{eq} 0.02 N_{ax} 0.48

α–LUMO -2.446	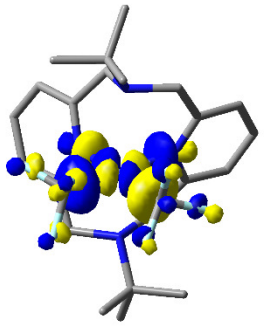	Ni 0.39 C_{CF3} 0.32 N_{eq} 0.13 N_{ax} 0.00
β-LUMO -3.156	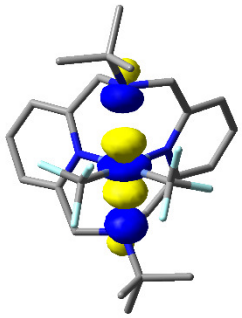	Ni 0.73 C_{CF3} 0.02 N_{eq} 0.01 N_{ax} 0.17
β-LUMO+1 -1.854	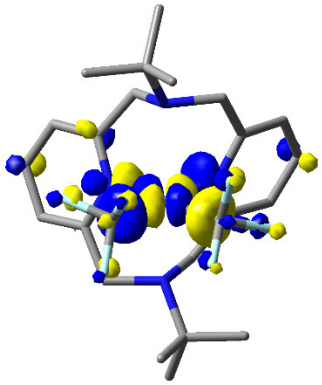	Ni 0.40 C_{CF3} 0.20 N_{eq} 0.15 N_{ax} 0.00

Table S5. TD-DFT calculated absorption bands and their composition for $[(^{Me}N4)Ni^{III}(CF_3)_2]^+$, **1**$^+$. Only the transitions with oscillator strengths greater than 0.001 are shown; the major contributing transitions have more than 10% contribution to the absorption band.

Wavelength (nm)	Oscillator strength	Major contributing transitions
580.4	0.0026	H-9(B)->LUMO(B) (71%), H-1(B)->LUMO(B) (14%)
553.9	0.0014	HOMO(A)->LUMO(A) (92%)
349.2	0.0029	H-4(A)->LUMO(A) (23%), H-6(A)->LUMO(A) (10%), H-9(B)->L+2(B) (10%)
332.8	0.001	HOMO(A)->L+1(A) (91%)
330.4	0.0024	H-3(B)->LUMO(B) (30%), H-5(A)->LUMO(A) (13%), H-7(B)->LUMO(B) (10%)
327.7	0.0012	H-1(A)->L+3(A) (17%), HOMO(B)->L+4(B) (15%), H-3(B)->LUMO(B) (13%)
315.0	0.1034	H-1(B)->LUMO(B) (76%), H-9(B)->LUMO(B) (11%)
310.2	0.0017	H-11(A)->LUMO(A) (34%), H-7(A)->LUMO(A) (28%), H-6(B)->L+2(B) (10%)
303.4	0.0028	H-1(A)->LUMO(A) (82%)

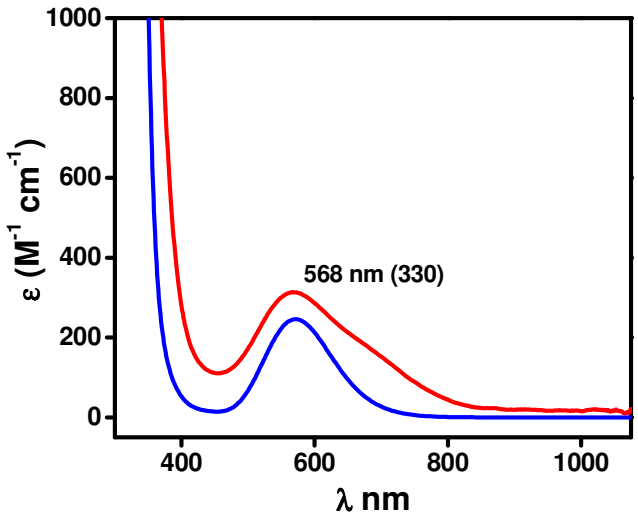

Figure S19. Comparison of the experimental and TD-DFT calculated UV-vis spectra of $[(^{Me}N4)Ni^{III}(CF_3)_2]^+$, **1**$^+$ (FWHM = 2500 cm^{-1}).

Table S6. TD-DFT calculated absorption bands and their composition for $[(^{tBu}N4)Ni^{III}(CF_3)_2]^+$, **2**$^+$. Only the transitions with oscillator strengths greater than 0.001 are shown; the major contributing transitions have more than 10% contribution to the absorption band.

Wavelength (nm)	Oscillator strength	Major contributing transitions
765.0	0.0037	H-12(B)->LUMO(B) (38%), H-10(B)->LUMO(B) (35%), HOMO(B)->LUMO(B) (10%)
456.6	0.0018	HOMO(A)->LUMO(A) (83%)
434.8	0.1068	HOMO(B)->LUMO(B) (86%)
399.5	0.0058	H-2(B)->LUMO(B) (32%), H-3(B)->LUMO(B) (20%), H-4(A)->LUMO(A) (12%), H-5(B)->LUMO(B) (11%)
398.6	0.0024	H-4(B)->LUMO(B) (61%), H-7(B)->LUMO(B) (14%)
378.7	0.0109	H-1(B)->LUMO(B) (96%)
370.0	0.0018	H-2(B)->LUMO(B) (35%), H-4(A)->LUMO(A) (16%), H-4(B)->L+1(B) (10%)
360.0	0.0012	H-5(B)->LUMO(B) (14%), H-13(A)->LUMO(A) (11%), H-12(B)->L+1(B) (10%)
337.8	0.0115	H-5(B)->LUMO(B) (41%), H-6(B)->LUMO(B) (13%)
312.5	0.0057	H-2(A)->LUMO(A) (18%), H-5(A)->LUMO(A) (14%), HOMO(B)->L+1(B) (11%)
312.3	0.0044	H-2(A)->LUMO(A) (22%), HOMO(B)->L+1(B) (13%), H-5(A)->LUMO(A) (10%),
306.7	0.0042	H-5(A)->LUMO(A) (19%), H-6(A)->LUMO(A) (17%), H-5(B)->L+1(B) (17%)

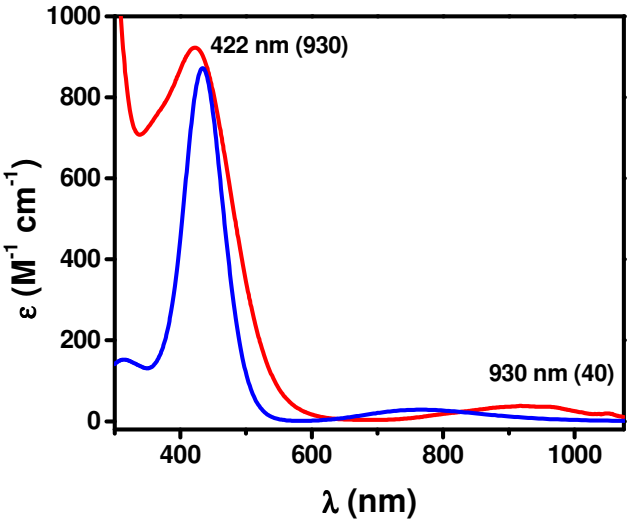

Figure S20. Comparison of the experimental and TD-DFT calculated UV-vis spectra of $[(^{tBu}N4)Ni^{III}(CF_3)_2]^+$, **2**$^+$ (FWHM = 2500 cm^{-1}).

Table S7. Comparison of DFT-calculated EPR parameters and experimental values.

Compound		g values			Superhyperfine coupling (G)
		g_x	g_y	g_z	$A(z,z)$
$[(^{tBu}N4)Ni^{III}(CF_3)_2]^+$ **1**$^+$	Expt	2.154	2.152	2.011	A_{2N} = 18.5
	DFT	2.138	2.136	2.021	A_{2N} = 17.5
$[(^{Me}N4)Ni^{III}(CF_3)_2]^+$ **2**$^+$	Expt	2.221	2.199	2.010	A_{2N} = 14.3
	DFT	2.183	2.172	2.022	A_{2N} = 14.4

VII. X-ray structure determination of 2, [2$^+$]PF6, and [1$^+$]PF6.

Diffraction-quality crystals of (^{tBu}N4)Ni^{II}(CF_3)$_2$, [(^{tBu}N4)Ni^{III}(CF_3)$_2$]PF_6, and [(^{Me}N4)Ni^{III}(CF_3)$_2$]PF_6 were obtained by pentane diffusion into THF solutions at –35 °C. Suitable crystals were mounted on MiTeGen cryoloops in random orientations in a Bruker Kappa Apex-II CCD X-ray diffractometer equipped with an Oxford Cryostream LT device and a fine focus Mo Kα radiation X-ray source (λ = 0.71073 Å). Preliminary unit cell constants were determined with a set of 36 narrow frame scans. Typical data sets consist of combinations of ϖ and ϕ scan frames with a typical scan width of 0.5° and a counting time of 15–30 s/frame at a crystal-to-detector distance of 3.5 cm. The collected frames were integrated using an orientation matrix determined from the narrow frame scans. Apex II and SAINT software packages (Bruker Analytical X-Ray, Madison, WI, 2008) were used for data collection and data integration. Analysis of the integrated data did not show any decay. Final cell constants were determined by global refinement of xyz centroids of reflections from the complete data sets. Collected data were corrected for systematic errors using SADABS (Bruker Analytical X-Ray, Madison, WI, 2008) based on the Laue symmetry using equivalent reflections. Structure solutions and refinement were carried out using the SHELXTL-PLUS software package. The structures were solved by direct methods and refined successfully. Full matrix least-squares refinements were carried out by minimizing $\Sigma w(Fo^2-Fc^2)^2$. The non-hydrogen atoms were refined anisotropically to convergence. The hydrogen atoms were treated using appropriate riding model.

b)

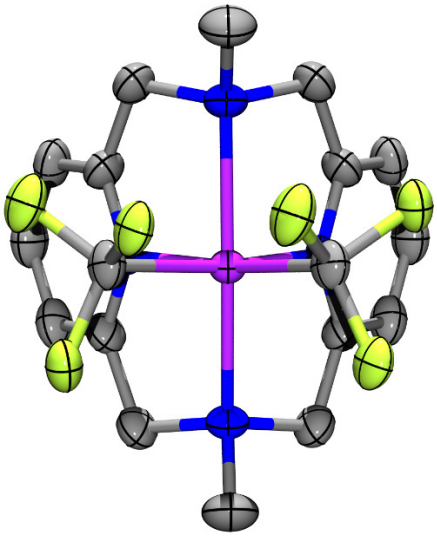

a)

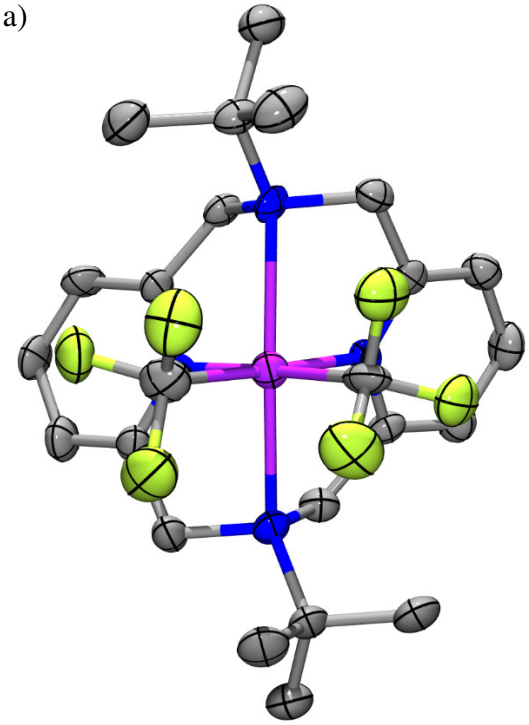

Figure S21. Front view of the ORTEP representations of the cations of [**1**$^{+}$]PF_6 (30% probability thermal ellipsoids) and [**2**$^{+}$]PF_6 (50% probability thermal ellipsoids).

Table S8. Crystal data and structure refinement for $[(^{Me}N4)Ni^{III}(CF_3)_2]PF_6$.

Identification code	l18913/lt/FT-112513-MeN4	
Empirical formula	$C_{18}\ H_{20}\ F_{12}\ N_4\ Ni\ P$	
Formula weight	610.06	
Temperature	100(2) K	
Wavelength	0.71073 Å	
Crystal system	Orthorhombic	
Space group	C mcm	
Unit cell dimensions	a = 10.3657(9) Å	α= 90°.
	b = 13.2968(11) Å	β= 90°.
	c = 16.2518(14) Å	γ = 90°.
Volume	2240.0(3) $Å^3$	
Z	4	
Density (calculated)	1.809 Mg/m^3	
Absorption coefficient	1.053 mm^{-1}	
F(000)	1228	
Crystal size	0.499 x 0.066 x 0.042 mm^3	
Theta range for data collection	2.491 to 25.417°.	
Index ranges	-10≤h≤12, -16≤k≤14, -19≤l≤19	
Reflections collected	13318	
Independent reflections	1136 [R(int) = 0.0477]	
Completeness to theta = 25.000°	99.4 %	
Absorption correction	Semi-empirical from equivalents	
Max. and min. transmission	0.8620 and 0.6661	
Refinement method	Full-matrix least-squares on F^2	
Data / restraints / parameters	1136 / 214 / 117	
Goodness-of-fit on F^2	1.100	
Final R indices [I>2sigma(I)]	R1 = 0.0859, wR2 = 0.2402	
R indices (all data)	R1 = 0.1004, wR2 = 0.2561	
Extinction coefficient	n/a	
Largest diff. peak and hole	1.298 and -0.724 $e.Å^{-3}$	

Table S9. Bond lengths [Å] for [(^{Me}N4)Ni^{III}(CF_3)$_2$]PF_6.

Ni(1)-C(6)	1.91(2)
Ni(1)-N(1)	1.962(7)
Ni(1)-N(1)#1	1.962(7)
Ni(1)-C(6')	2.014(19)
Ni(1)-N(2)	2.212(8)
Ni(1)-N(2)#2	2.212(8)
N(1)-C(1)#3	1.322(8)
N(1)-C(1)	1.322(8)
N(2)-C(5)	1.467(14)
N(2)-C(4)	1.473(8)
N(2)-C(4)#1	1.473(8)
C(1)-C(2)	1.395(11)
C(1)-C(4)	1.495(11)
C(2)-C(3)	1.346(11)
C(2)-H(2)	0.9500
C(3)-C(2)#3	1.346(11)
C(3)-H(3)	0.9500
C(4)-H(4A)	0.9900
C(4)-H(4B)	0.9900
C(5)-H(5A)	0.9800
C(5)-H(5B)	0.9800
C(5)-H(5C)	0.9800
C(6)-F(2)	1.368(9)
C(6)-F(3)	1.370(9)
C(6)-F(1)	1.378(9)
C(6')-F(3')	1.370(9)
C(6')-F(1')	1.371(9)
C(6')-F(2')	1.374(9)
P(1)-F(4)#4	1.552(6)
P(1)-F(4)	1.552(6)
P(1)-F(5)	1.565(5)
P(1)-F(5)#4	1.565(5)

P(1)-F(5)#5	1.565(5)
P(1)-F(5)#6	1.565(5)

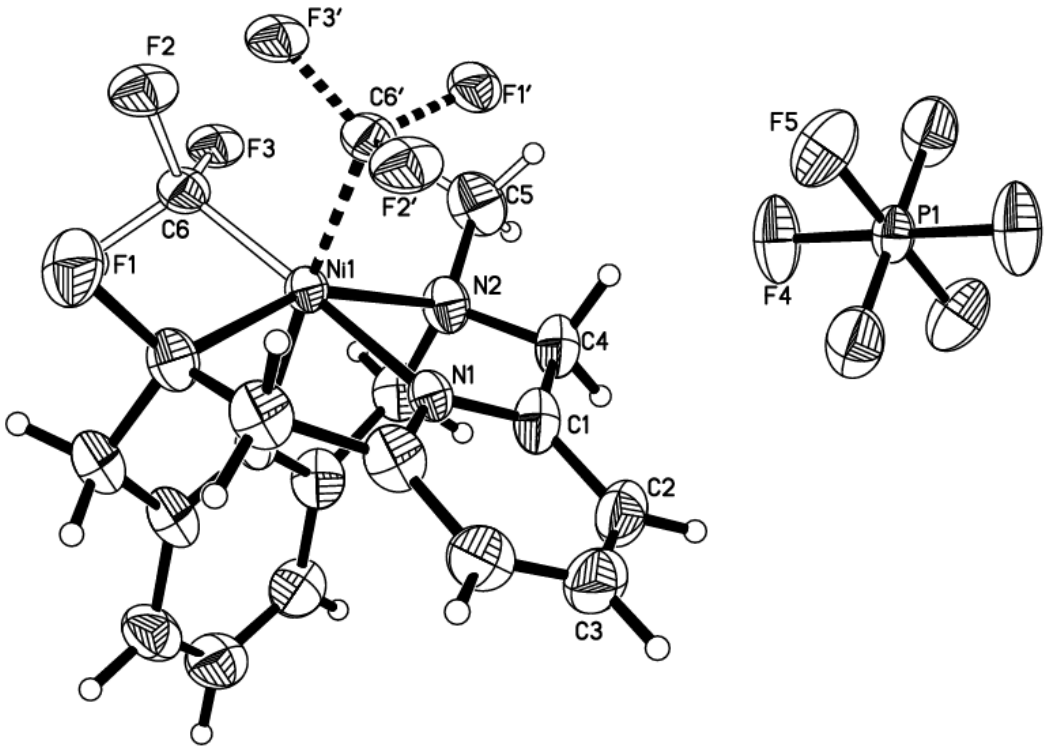

Figure S22. Projection view with 30% probability ellipsoids for $[(^{Me}N4)Ni^{III}(CF_3)_2]PF_6$.

Table S10. Crystal data and structure refinement for (^{tBu}N4)Ni^{II}(CF_3)$_2$.

Identification code	l111513lt/x8/Ft-070813-2(yellow rod)	
Empirical formula	C_{53} H_{76} F_{12} N_8 Ni_2	
Formula weight	1170.63	
Temperature	100(2) K	
Wavelength	0.71073 Å	
Crystal system	Monoclinic	
Space group	P 2_1/n	
Unit cell dimensions	a = 10.2621(5) Å	α= 90°.
	b = 19.5073(8) Å	β= 96.154(3)°.
	c = 13.4730(6) Å	γ = 90°.
Volume	2681.6(2) Å^3	
Z	2	
Density (calculated)	1.450 Mg/m^3	
Absorption coefficient	0.788 mm^{-1}	
F(000)	1228	
Crystal size	0.274 x 0.161 x 0.057 mm^3	
Theta range for data collection	1.844 to 25.452°.	
Index ranges	-12≤h≤12, -21≤k≤23, -16≤l≤16	
Reflections collected	41249	
Independent reflections	4944 [R(int) = 0.0726]	
Completeness to theta = 25.242°	100.0 %	
Absorption correction	Semi-empirical from equivalents	
Max. and min. transmission	0.7452 and 0.6552	
Refinement method	Full-matrix least-squares on F^2	
Data / restraints / parameters	4944 / 168 / 368	
Goodness-of-fit on F^2	1.019	
Final R indices [I>2sigma(I)]	R1 = 0.0384, wR2 = 0.0816	
R indices (all data)	R1 = 0.0610, wR2 = 0.0905	
Extinction coefficient	n/a	
Largest diff. peak and hole	0.724 and -0.407 e.Å^{-3}	

Table S11. Bond lengths [Å] for (^{tBu}N4)Ni^{II}(CF_3)$_2$.

Ni(1)-C(23)	1.905(3)	C(6)-H(6A)	0.9900
Ni(1)-C(24)	1.915(3)	C(6)-H(6B)	0.9900
Ni(1)-N(1)	1.939(2)	C(7)-C(8)	1.504(4)
Ni(1)-N(2)	1.994(2)	C(7)-H(7A)	0.9900
F(1)-C(23)	1.372(3)	C(7)-H(7B)	0.9900
F(2)-C(23)	1.365(3)	C(8)-C(9)	1.393(4)
F(3)-C(23)	1.358(3)	C(9)-C(10)	1.377(4)
F(4)-C(24)	1.437(4)	C(9)-H(9)	0.9500
F(5)-C(24)	1.341(4)	C(10)-C(11)	1.380(4)
F(6)-C(24)	1.348(5)	C(10)-H(10)	0.9500
F(4')-C(24)	1.338(4)	C(11)-C(12)	1.381(4)
F(5')-C(24)	1.433(4)	C(11)-H(11)	0.9500
F(6')-C(24)	1.328(5)	C(12)-C(13)	1.504(4)
N(1)-C(1)	1.351(3)	C(13)-H(13A)	0.9900
N(1)-C(5)	1.352(3)	C(13)-H(13B)	0.9900
N(2)-C(8)	1.340(3)	C(14)-H(14A)	0.9900
N(2)-C(12)	1.353(3)	C(14)-H(14B)	0.9900
N(3)-C(7)	1.466(3)	C(15)-C(16)	1.525(4)
N(3)-C(6)	1.472(3)	C(15)-C(17)	1.529(4)
N(3)-C(15)	1.505(3)	C(15)-C(18)	1.532(4)
N(4)-C(14)	1.468(3)	C(16)-H(16A)	0.9800
N(4)-C(13)	1.477(3)	C(16)-H(16B)	0.9800
N(4)-C(19)	1.495(3)	C(16)-H(16C)	0.9800
C(1)-C(2)	1.388(3)	C(17)-H(17A)	0.9800
C(1)-C(14)	1.514(3)	C(17)-H(17B)	0.9800
C(2)-C(3)	1.381(4)	C(17)-H(17C)	0.9800
C(2)-H(2)	0.9500	C(18)-H(18A)	0.9800
C(3)-C(4)	1.375(4)	C(18)-H(18B)	0.9800
C(3)-H(3)	0.9500	C(18)-H(18C)	0.9800
C(4)-C(5)	1.387(4)	C(19)-C(20)	1.528(4)
C(4)-H(4)	0.9500	C(19)-C(21)	1.528(4)
C(5)-C(6)	1.502(4)	C(19)-C(22)	1.532(4)

C(20)-H(20A)	0.9800	C(4S)-H(4S2)	0.9900
C(20)-H(20B)	0.9800	C(5S)-H(5S1)	0.9800
C(20)-H(20C)	0.9800	C(5S)-H(5S2)	0.9800
C(21)-H(21A)	0.9800	C(5S)-H(5S3)	0.9800
C(21)-H(21B)	0.9800	C(1S')-C(2S')	1.5229
C(21)-H(21C)	0.9800	C(1S')-H(1S4)	0.9800
C(22)-H(22A)	0.9800	C(1S')-H(1S5)	0.9800
C(22)-H(22B)	0.9800	C(1S')-H(1S6)	0.9800
C(22)-H(22C)	0.9800	C(2S')-C(3S')	1.6378
C(1S)-C(2S)	1.5333	C(2S')-H(2S3)	0.9900
C(1S)-H(1S1)	0.9800	C(2S')-H(2S4)	0.9900
C(1S)-H(1S2)	0.9800	C(3S')-C(4S')	1.4866
C(1S)-H(1S3)	0.9800	C(3S')-H(3S3)	0.9900
C(2S)-C(3S)	1.6368	C(3S')-H(3S4)	0.9900
C(2S)-H(2S1)	0.9900	C(4S')-C(5S')	1.6047
C(2S)-H(2S2)	0.9900	C(4S')-H(4S3)	0.9900
C(3S)-C(4S)	1.4675	C(4S')-H(4S4)	0.9900
C(3S)-H(3S1)	0.9900	C(5S')-H(5S4)	0.9800
C(3S)-H(3S2)	0.9900	C(5S')-H(5S5)	0.9800
C(4S)-C(5S)	1.6066	C(5S')-H(5S6)	0.9800
C(4S)-H(4S1)	0.9900		

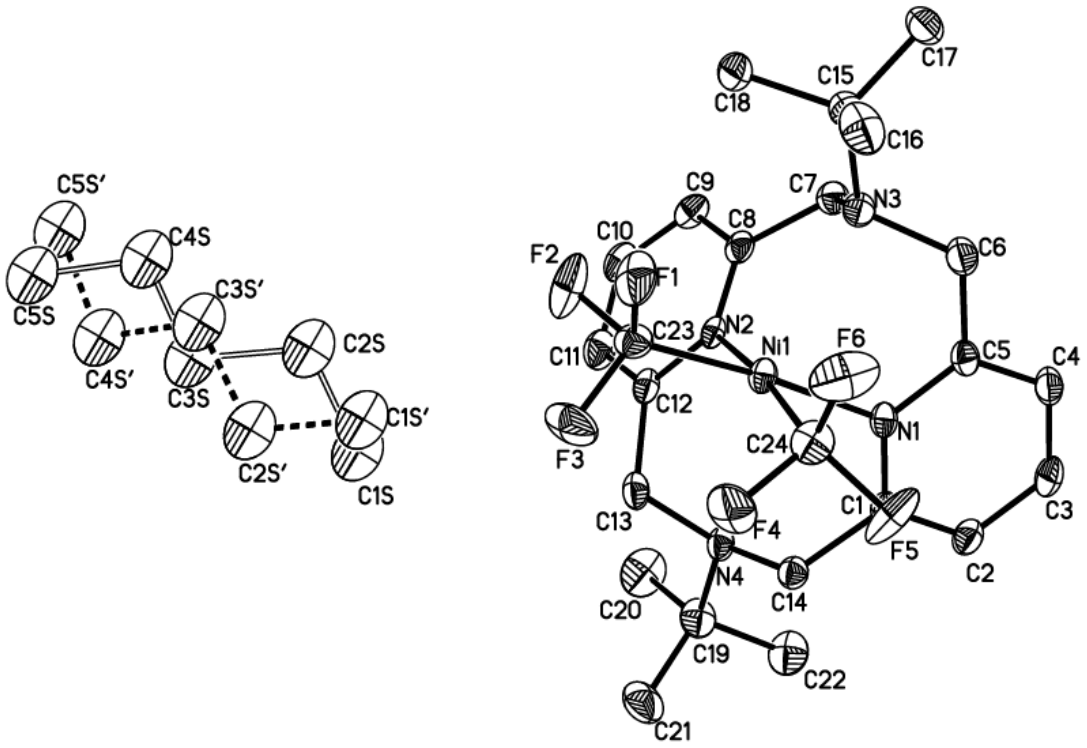

Figure S23. Projection view with 50% probability for (^{tBu}N4)Ni^{II}(CF$_3$)$_2$.

Table S12. Crystal data and structure refinement for $[(^{tBu}N4)Ni^{III}(CF_3)_2]PF_6$.

Identification code	l11613/lt/x8/FT070813-1B	
Empirical formula	C_{28} H_{40} F_{12} N_4 Ni O P	
Formula weight	766.32	
Temperature	100(2) K	
Wavelength	0.71073 Å	
Crystal system	Orthorhombic	
Space group	P b c a	
Unit cell dimensions	a = 14.2479(13) Å	α= 90°.
	b = 14.4930(15) Å	β= 90°.
	c = 30.515(3) Å	γ = 90°.
Volume	6301.2(11) $Å^3$	
Z	8	
Density (calculated)	1.616 Mg/m^3	
Absorption coefficient	0.769 mm^{-1}	
F(000)	3160	
Crystal size	0.241 x 0.239 x 0.109 mm^3	
Theta range for data collection	1.956 to 24.998°.	
Index ranges	-16≤h≤16, -17≤k≤17, -36≤l≤36	
Reflections collected	123227	
Independent reflections	5548 [R(int) = 0.3433]	
Completeness to theta = 25.000°	99.9 %	
Absorption correction	Semi-empirical from equivalents	
Max. and min. transmission	0.7440 and 0.6363	
Refinement method	Full-matrix least-squares on F^2	
Data / restraints / parameters	5548 / 46 / 430	
Goodness-of-fit on F^2	1.006	
Final R indices [I>2sigma(I)]	R1 = 0.0647, wR2 = 0.1380	
R indices (all data)	R1 = 0.1687, wR2 = 0.1906	
Extinction coefficient	n/a	
Largest diff. peak and hole	0.686 and -0.766 $e.Å^{-3}$	

Table S13. Bond lengths [Å] for $[(^{tBu}N4)Ni^{III}(CF_3)_2]PF_6$.

Ni(1)-N(2)	1.924(5)	C(7)-H(7A)	0.9900
Ni(1)-N(1)	1.946(5)	C(7)-H(7B)	0.9900
Ni(1)-C(24)	1.949(8)	C(8)-C(9)	1.369(9)
Ni(1)-C(23)	1.969(8)	C(9)-C(10)	1.377(10)
Ni(1)-N(4)	2.399(5)	C(9)-H(9)	0.9500
Ni(1)-N(3)	2.431(6)	C(10)-C(11)	1.396(10)
F(1)-C(23)	1.341(9)	C(10)-H(10)	0.9500
F(2)-C(23)	1.353(8)	C(11)-C(12)	1.381(9)
F(3)-C(23)	1.392(9)	C(11)-H(11)	0.9500
F(4)-C(24)	1.333(8)	C(12)-C(13)	1.481(9)
F(5)-C(24)	1.354(8)	C(13)-H(13A)	0.9900
F(6)-C(24)	1.367(8)	C(13)-H(13B)	0.9900
N(1)-C(1)	1.334(8)	C(14)-H(14A)	0.9900
N(1)-C(5)	1.347(8)	C(14)-H(14B)	0.9900
N(2)-C(8)	1.341(8)	C(15)-C(16)	1.504(10)
N(2)-C(12)	1.351(8)	C(15)-C(17)	1.533(11)
N(3)-C(6)	1.480(9)	C(15)-C(18)	1.535(10)
N(3)-C(7)	1.495(9)	C(16)-H(16A)	0.9800
N(3)-C(15)	1.556(8)	C(16)-H(16B)	0.9800
N(4)-C(14)	1.495(8)	C(16)-H(16C)	0.9800
N(4)-C(13)	1.516(8)	C(17)-H(17A)	0.9800
N(4)-C(19)	1.531(8)	C(17)-H(17B)	0.9800
C(1)-C(2)	1.377(9)	C(17)-H(17C)	0.9800
C(1)-C(14)	1.495(9)	C(18)-H(18A)	0.9800
C(2)-C(3)	1.383(10)	C(18)-H(18B)	0.9800
C(2)-H(2)	0.9500	C(18)-H(18C)	0.9800
C(3)-C(4)	1.391(10)	C(19)-C(22)	1.523(10)
C(3)-H(3)	0.9500	C(19)-C(20)	1.525(10)
C(4)-C(5)	1.371(9)	C(19)-C(21)	1.536(10)
C(4)-H(4)	0.9500	C(20)-H(20A)	0.9800
C(5)-C(6)	1.509(9)	C(20)-H(20B)	0.9800
C(6)-H(6A)	0.9900	C(20)-H(20C)	0.9800
C(6)-H(6B)	0.9900	C(21)-H(21A)	0.9800
C(7)-C(8)	1.511(9)	C(21)-H(21B)	0.9800

C(21)-H(21C)	0.9800	C(1S)-C(2S)	1.504(18)
C(22)-H(22A)	0.9800	C(1S)-H(1S1)	0.9900
C(22)-H(22B)	0.9800	C(1S)-H(1S2)	0.9900
C(22)-H(22C)	0.9800	C(2S)-C(3S)	1.507(12)
P(1)-F(7)	1.569(5)	C(2S)-H(2SA)	0.9900
P(1)-F(11)	1.574(5)	C(2S)-H(2SB)	0.9900
P(1)-F(10)	1.581(4)	C(3S)-C(4S)	1.519(12)
P(1)-F(8)	1.581(5)	C(3S)-H(3SA)	0.9900
P(1)-F(9)	1.592(5)	C(3S)-H(3SB)	0.9900
P(1)-F(12)	1.596(5)	C(4S)-H(4S1)	0.9900
O(1S)-C(1S)	1.355(14)	C(4S)-H(4S2)	0.9900
O(1S)-C(4S)	1.366(11)		

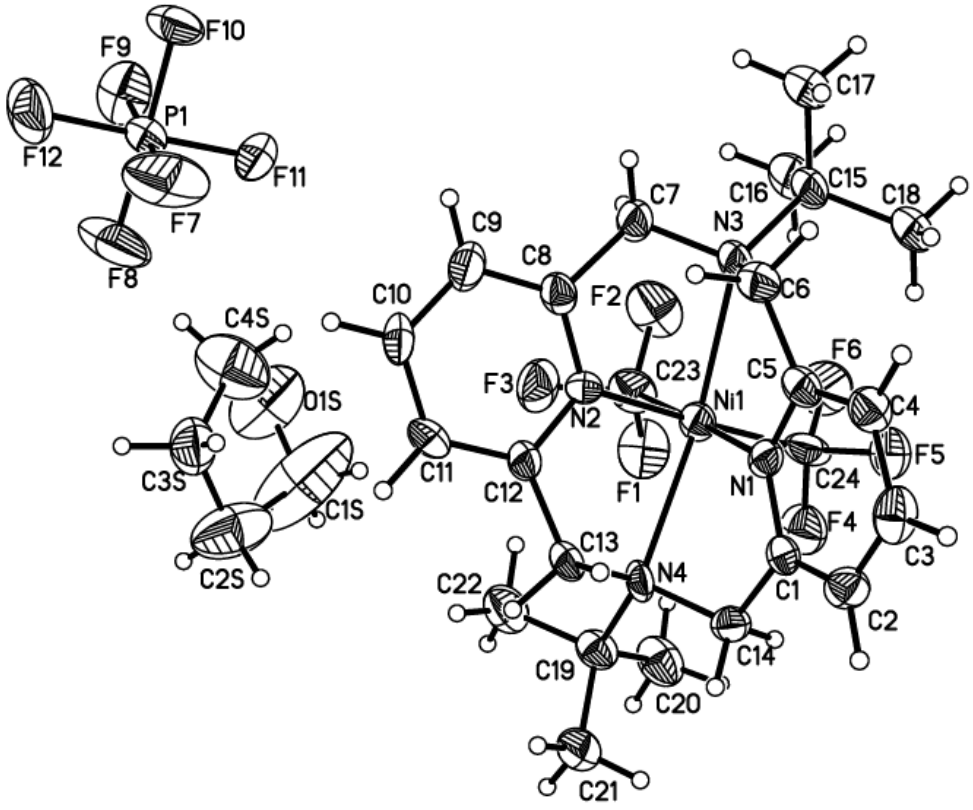

Figure S24. Projection view with 50% probability ellipsoids for $[(^{tBu}N4)Ni^{III}(CF_3)_2]PF_6$.

VIII. References

1. Zhang, C. P.; Wang, H.; Klein, A.; Biewer, C.; Stimat, K.; Yarnaguchi, Y.; Xu, L.; Gomez-Benitez, V.; Vicic, D. A. *J. Am. Chem. Soc.* **2013**, *135*, 8141.
2. Fulmer, G. R.; Miller, A. J. M.; Sherden, N. H.; Gottlieb, H. E.; Nudelman, A.; Stoltz, B. M.; Bercaw, J. E.; Goldberg, K. I. *Organometallics* **2010**, *29*, 2176.
3. Evans, D. F. *J. Chem. Soc.* **1959**, 2003.
4. a) De Buysser, K.; Herman, G. G.; Bruneel, E.; Hoste, S.; Van Driessche, I. *Chem. Phys.* **2005**, *315*, 286; b) Bain, G. A.; Berry, J. F. *J. Chem. Educ.* **2008**, *85*, 532.
5. a) Sartori, P.; Habel, W. *J. Fluorine Chem.* **1980**, *16*, 265; b) Bhadury, P. S.; Singh, S.; Sharma, M.; Palit, M. *J. Anal. Appl. Pyrolysis* **2007**, *78*, 288.
6. M. J. Frisch, G. W. T., H. B. Schlegel, G. E. Scuseria, M. A. Robb, J. R. Cheeseman, G. Scalmani, V. Barone, B. Mennucci, G. A. Petersson, H. Nakatsuji, M. Caricato, X. Li, H. P. Hratchian, A. F. Izmaylov, J. Bloino, G. Zheng, J. L. Sonnenberg, M. Hada, M. Ehara, K. Toyota, R. Fukuda, J. Hasegawa, M. Ishida, T. Nakajima, Y. Honda, O. Kitao, H. Nakai, T. Vreven, J. A. Montgomery, Jr., J. E. Peralta, F. Ogliaro, M. Bearpark, J. J. Heyd, E. Brothers, K. N. Kudin, V. N. Staroverov, R. Kobayashi, J. Normand, K. Raghavachari, A. Rendell, J. C. Burant, S. S. Iyengar, J. Tomasi, M. Cossi, N. Rega, J. M. Millam, M. Klene, J. E. Knox, J. B. Cross, V. Bakken, C. Adamo, J. Jaramillo, R. Gomperts, R. E. Stratmann, O. Yazyev, A. J. Austin, R. Cammi, C. Pomelli, J. W. Ochterski, R. L. Martin, K. Morokuma, V. G. Zakrzewski, G. A. Voth, P. Salvador, J. J. Dannenberg, S. Dapprich, A. D. Daniels, O. Farkas, J. B. Foresman, J. V. Ortiz, J. Cioslowski, D. J. Fox, *Gaussian 09, Revision A.02*, Gaussian, Inc., Wallingford CT, **2009**.
7. Lee, C. M.; Chen, C. H.; Liao, F. X.; Hu, C. H.; Lee, G. H. *J. Am. Chem. Soc.* **2010**, *132*, 9256.
8. Neese, F. *Wiley Interdiscip. Rev.: Comput. Mol. Sci.* **2012**, *2*, 73.